Numerical Investigation of Cold-Formed Stainless Steel Lipped Channels with Longitudinal Stiffeners Subjected to Shear

D. M. M. P. Dissanayake
Faculty of Engineering and Environment, University of Northumbria,
Newcastle, UK.
K. Poologanathan
Faculty of Engineering and Environment, University of Northumbria,
Newcastle, UK.
S. Gunalan
School of Engineering and Built Environment, Griffith University,
Gold Coast, Australia.
K. D. Tsavdaridis
School of Civil Engineering, Faculty of Engineering and Physical Sciences, University of Leeds, UK.
K. S. Wanniarachchi
Faculty of Engineering, University of Ruhuna, Sri Lanka.
B. Nagaratnam
Faculty of Engineering and Environment, University of Northumbria,
Newcastle, UK.

Abstract

The shear response of the cold-formed stainless steel lipped channel sections with longitudinal stiffeners has not been investigated adequately in the past. Therefore, this paper presents the details of numerical investigations conducted to study the shear behaviour of longitudinally stiffened cold-formed stainless steel lipped channel sections. Following a validation study of the finite element models of lipped channel sections, the effect of return lips and web stiffeners on the shear response of lipped channel sections was examined through comprehensive numerical parametric studies. In addition, numerical investigations were conducted to study the elastic shear buckling response of the sections and the shear buckling coefficients were back-calculated. It was found that the longitudinal web stiffeners enhance the shear buckling resistance of lipped channel sections considerably with increased stiffener depth. However, the shear capacity increment is not significant compared to plain lipped channel sections. The presence of the web stiffeners is found to be not preventing the out-of-plane buckling of the sections. The evaluation of Eurocode 3 and the direct strength method shear provisions for stainless steel channel sections with longitudinal stiffeners illustrated inaccurate capacity predictions. Therefore, modifications were proposed and comparisons reveal that the proposed provisions enhance the shear resistance predictions with good accuracy over the codified provisions.

Keywords: Cold-formed stainless steel, Channel sections, Longitudinal stiffeners, Shear and shear buckling, Eurocode 3, Direct strength method

1 Introduction

Cold-formed sections are commonly used in the construction industry and can be found in a wider range of applications as structural components such as roof purlins, wall studs and floor joists. This is mainly because the cold-forming manufacturing techniques such as roll forming and press braking have made it possible to produce cold-formed sections of high strength-to-weight ratio. In addition to commonly available cold-formed sections such as C-sections, Z-sections and hollow sections, complex cross-sectional geometries feature longitudinal stiffeners to enhance their structural performance. Over the years, many research studies have been conducted to investigate the structural behaviour of cold-formed steel stiffened sections. Pham et al. [1] conducted experimental studies on cold-formed steel channel sections with trapezoidal and rectangular web stiffeners subjected primarily to shear action. Pham and Hancock [2] tested plain and SupaCee® channel sections for shear, and combined bending and shear actions. Wang and Young [3] investigated the bending behaviour of cold-formed steel channel sections with stiffened webs using experiments. Furthermore, Pham et al. [4] conducted numerical studies on the shear behaviour of cold-formed steel channel sections with rectangular and triangular web stiffeners. However, less attention has been given on the cold-formed stainless steel stiffened sections in the past. Therefore, this paper aims to investigate the shear response of cold-formed stainless steel channel sections with longitudinal stiffeners using numerical studies.

For the design of stainless steel sections, European standards for stainless steel, EN1993-1-4 [5] is available and should be referred with European standards for plated structural elements, EN1993-1-5 [6]. In the current version of EN1993-1-5 [6], Höglund’s [7] rotated stress field theory is adopted to calculate the shear buckling resistance of sections with both stiffened and unstiffened webs and takes into account the flange contribution to the shear resistance. However, European standards neglect the beneficial effect of element interaction in the calculation of section resistance [8]. Alternatively, the direct strength method (DSM) and the continuous strength method (CSM) have recently been introduced for the design of steel sections. Both these design approaches deal with the full cross-section buckling, therefore taking into consideration the element interaction to the section resistance. When calculating the full cross-section buckling resistance, numerical techniques such as finite strip method (FSM) and finite element method (FEM) may be associated. The FSM is adopted in software such as CUFSM [9] and THIN-WALL-2 [10] while there are many commercially available software packages for FEM. The DSM of design for shear is recently introduced in Australian/New Zealand standards, AS/NZS 4600 [11] and American specifications, AISI S100 [12] for cold-formed steel design.

In this paper, the details of numerical simulations conducted to investigate the shear behaviour and the elastic shear buckling behaviour of cold-formed stainless steel channel sections with longitudinal stiffeners is presented. Based on the numerical results, a set of equations for both EN1993-1-4 [5] and the DSM was proposed to predict the shear resistance of cold-formed stainless steel stiffened channel sections.

2 Finite element (FE) modelling of shear behaviour

The shear behaviour of cold-formed stainless steel lipped channel beams (LCBs) were first simulated using commercially available FE software package ABAQUS CAE 2017 and the details of numerical modelling are given in this section. The developed FE models are based on the three-point loading tests of cold-formed stainless steel LCBs found in Dissanayake et al. [13]. FE models were developed for eight tests of LCBs with an aspect ratio (shear span (a) to clear web depth (d_1) ratio) of 1.0. Keerthan and Mahendran [14] showed that when shorter spans (with a/d_1=1.0) are employed in the shear tests, the generated bending moments are of lower magnitudes, thus no bending-shear interaction is taken place within the sections. Therefore, this aspect ratio ensures that the shear stresses generated within the sections are independent of bending stresses. In the experiments, the back-to-back beam arrangement has been employed to eliminate torsional effects, however, single LCBs were modelled together with three web side plates in the numerical modelling considering the symmetry of the test setup. More details on the three-point loading tests and the back-to-back beam setups can be found in [14] for cold-formed steel LCBs and in [15]–[17] for cold-formed steel LiteSteel beams.

2.1 Element type and FE mesh

Four node shell element type with reduced integration (S4R) was chosen from Abaqus element library to model sections. This S4R shell element type has six degrees of freedom (DOFs) at each of its node. The element is ideal for large strain analyses since it accounts for finite membrane strains and large rotations [18]. A number of studies have previously proven the successful employment of this element type to simulate the non-linear behaviour of thin sections [19]–[23]. Mesh sensitivity analyses were conducted and convergence was identified which provides reasonably accurate results. The sensitivity analyses suggested a 5 mm × 5 mm mesh for flat parts of the sections. A relatively finer mesh of 1 mm × 5 mm was employed for corner regions to model the corner curvature. A coarser mesh of 10 mm × 10 mm was assigned to the web side plates as the attention was given to the steel sections. Fig. 1 illustrates the assembly of different parts and FE mesh employed in the analyses.

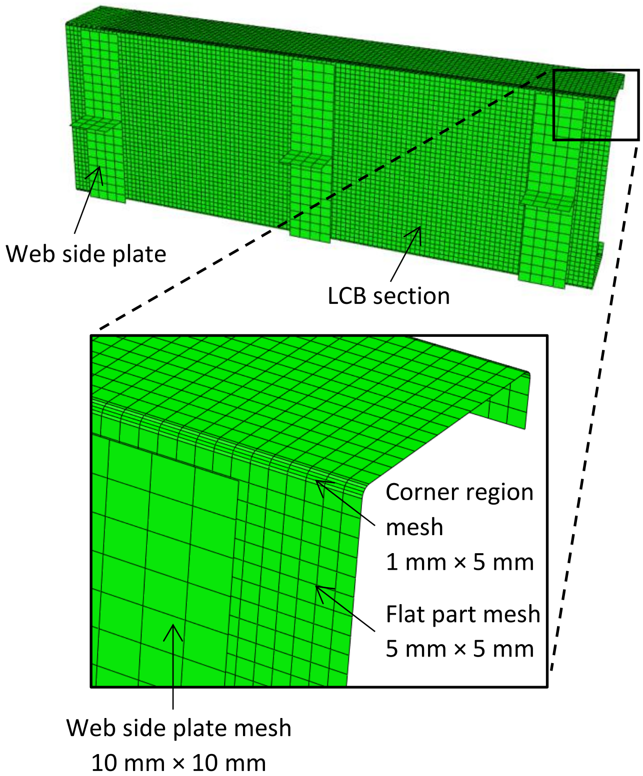

Fig. 1 Assembly of parts and FE mesh used in the modelling

2.2 Material modelling of stainless steel

Stainless steel exhibits a non-linear stress-strain behaviour with gradual yielding and shows different levels of strain hardening under higher strain levels in each stainless steel grade. To represent this non-linear material behaviour, two-stage Ramberg-Osgood material model has been widely used and a number of modifications have been proposed to the original version of this model. A recent study by Arrayago et al. [24] proposed modifications to the codified version of the two-stage Ramberg-Osgood model provided in EN1993-1-4 [5] considering a large number of stainless steel material data. The two-stage Ramberg-Osgood material model with Arrayago et al.'s [24] proposals was utilised to represent the stress-strain behaviour of stainless steel in numerical parametric studies conducted in Section 4 of this study. It is required to input stress-strain data of a non-linear material in terms of true stress (σ_{true}) and log plastic strain ($\varepsilon_{ln}{}^{pl}$) into Abaqus. Therefore, Eqs. (1) and (2) were used to calculate true stress (σ_{true}) and log plastic strain ($\varepsilon_{ln}{}^{pl}$) values of each stainless steel grade, respectively. A sufficient number of data sets were fed into Abaqus to accurately model the non-linear material behaviour.

$$\sigma_{true} = \sigma_{nom}(1 + \varepsilon_{nom}) \tag{1}$$

$$\varepsilon_{ln}^{pl} = \ln(1 + \varepsilon_{nom}) - \frac{\sigma_{true}}{E} \tag{2}$$

where σ_{nom} and ε_{nom} are the engineering stress and strain, respectively and E is Young's modulus.

During the cold-forming process of LCB sections, corner regions undergo plastic deformations. This leads to a change in material properties, typically associated with enhanced yield and ultimate stresses. These strength enhancements were explicitly included in the FE modelling of cold-formed stainless steel LCBs. Cruise and Gardner's [25] predictive model for enhanced corner 0.2 % proof stress and Ashraf et al.'s [26] proposal for enhanced corner ultimate stress were employed in Section 4 of this study. More details can be found from Dissanayake et al. [13].

2.3 Boundary conditions and loading

Boundary conditions were assigned to the FE models such that they accurately simulate the experimental conditions. Simply supported boundary conditions were maintained at the two beam ends by employing pin and roller support conditions to the end web side plates. This was achieved by restraining in-plane translational DOFs in the x-y plane at both these locations and restraining translational DOF in the z-direction at the left support. Further, rotational DOF about the longitudinal axis (z-axis) of the LCB was restrained at these two supports to eliminate any torsional effect. Lateral deflection along the x-axis and the rotation about the z-axis were fixed at the respective flange locations to simulate the effect of equal angle straps employed in the experiments to avoid distortional buckling of the sections. Mid-span loading was applied to the mid web side plate in terms of vertical downward displacement. The interaction between LCB web and web side plates due to the bolted connections was modelled by choosing tie constraints from Abaqus. Fig. 2 shows the locations of assigned boundary conditions in the FE modelling.

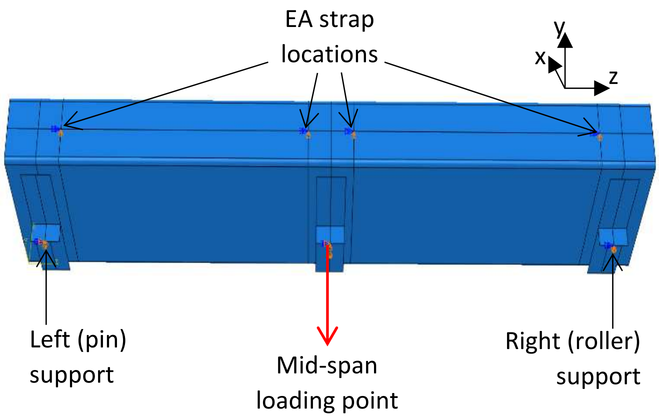

Fig. 2 Locations of the assigned boundary conditions in the FE modelling

2.4 Local geometric imperfections

The local or global deviations of the section geometry compared to its perfect geometry are called geometric imperfections. These imperfections can affect the performance of the structure. Therefore, geometric imperfection patterns were identified through numerical analyses and included in non-linear FE models using a suitable scaling factor. There were no signs of lateral torsional buckling of the sections observed in the experiments conducted by Dissanayake et al. [13]. Therefore, only the local geometric imperfections were taken into account in this study. Dawson and Walker [27] proposed a model for imperfection magnitude (ω_0) and this has been modified by Gardner and Nethercot [28]. This is given in Eq. (3) and was employed in this study to calculate the scaling factor.

$$\omega_0 = 0.023\left(\frac{\sigma_{0.2}}{\sigma_{cr}}\right)t \tag{3}$$

where $\sigma_{0.2}$ is the 0.2 % proof stress of the material, σ_{cr} is the lowest value of the critical elastic buckling stress calculated for the constituent plate elements of the section and t is the thickness.

2.5 Eigenvalue buckling analysis

An Eigenvalue buckling analysis was performed on each FE model to obtain the elastic buckling mode shapes of the section under the applied boundary conditions and loading patterns. From the generated buckling modes, critical buckling mode shapes were identified which are usually corresponding to the lowest Eigenmodes. These elastic buckling modes were taken as the initial geometric imperfection patterns of the sections and incorporated to perturb the section geometry in the non-linear analyses. Inputs to extract the relevant elastic buckling mode shapes with suitable scaling factors were given through command lines as instructed in user manuals [18].

2.6 Geometrically and materially non-linear analysis

A modified Static, Riks analysis was performed on the developed FE models to study the collapse mechanism and post-buckling response of the sections with due consideration giving to geometrically and materially non-linear effects. The effects of initial geometric imperfections were also added in the non-linear analysis to perturb the mesh. Subsequently, the ultimate loads of the sections at the failure were obtained from the load-displacement curves and the structural response of the sections was studied.

3 Validation of FE models for shear behaviour

The results obtained from the FE models of cold-formed stainless steel LCB sections which subjected to shear were compared with the experimental results of corresponding tests found from Dissanayake et al. [13]. The details of these comparisons are elaborated in this section. The measured geometric and material properties were utilised in the FE models developed for validation. Table 1 compares the experimental and FE ultimate shear capacities ($V_{Exp.}$ and V_{FE}). The format, section name followed by section depth (D) × section breadth (B) × lip height (L) × thickness (t) was adopted throughout this paper to designate the sections. From the results, it can be seen that the mean and the coefficient of variation (COV) of the experimental shear capacity to the FE shear capacity ratio are 1.02 and 0.073, respectively. Therefore, it can be concluded that the developed FE models predict the shear capacity of LCB sections with reasonably good accuracy.

Table 1 Experimental [13] and FE shear capacities for cold-formed stainless steel LCBs

LCB section	$V_{Exp.}$ (kN)	V_{FE} (kN)	$V_{Exp.}/V_{FE}$
LCB 100×50×15×1.2	18.49	16.86	1.10
LCB 100×50×15×1.5	24.44	23.90	1.02
LCB 100×50×15×2.0	36.00	32.72	1.10
LCB 150×65×15×1.2	21.60	20.09	1.08
LCB 150×65×15×1.5	26.26	28.40	0.92
LCB 150×65×15×2.0	43.55	42.60	1.02
LCB 200×75×15×1.2	22.98	22.97	1.00
LCB 200×75×15×2.0	47.05	52.11	0.90
Mean			1.02
COV			0.073

Further, experimental and FE shear failure modes were compared in Fig. 3. From Fig. 3, it is seen that the FE model is able to capture the diagonal shear failure of both webs in a fairly similar manner to the experimental failure mode. Therefore, it can be concluded that the shear behaviour of cold-formed stainless steel LCBs is well captured from these numerical models.

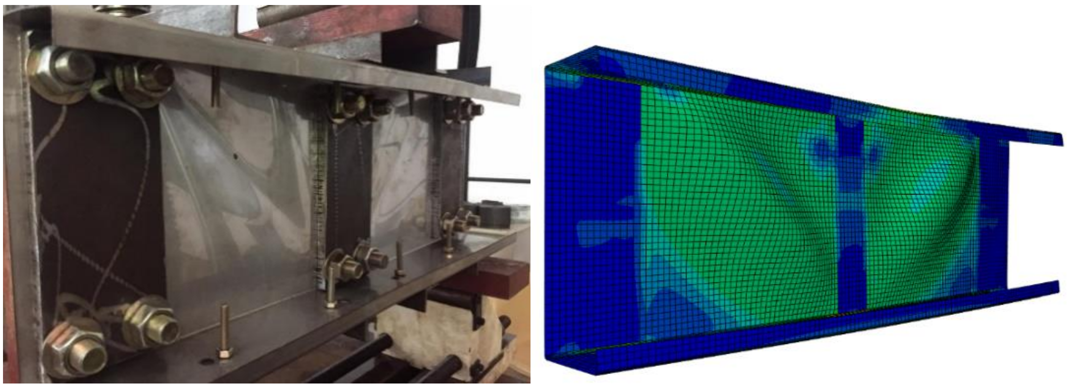

(a) (b)

Fig. 3 (a) Experimental [13] and (b) FE shear failure modes of cold-formed stainless steel LCB 200×75×15×1.2 section

4 Parametric study

4.1 General

The validated FE models of cold-formed stainless steel LCBs were then utilised in investigating the effect of different key parameters on the shear response of cold-formed stainless steel stiffened sections. Different types of longitudinal stiffeners were introduced to the LCB sections in the numerical modelling to accomplish this task. The details of cross-sections investigated herein are given in Fig. 4 alongside the key dimensions of a LCB section. In Fig. 4, the overall depth of the stiffeners is shown. The first section (LCB-RL) to study was a LCB section with return lips. The considered return lips were equal in length to lip depth. The second section (LCB-TR) was a LCB section with two triangular web stiffeners placed at one fourth and three fourths of the web height. Each triangular stiffener was 6 mm in height and 5 mm in depth. The third section (LCB-TP) was similar to the second one but trapezoidal web stiffeners were employed instead of triangular stiffeners. Each trapezoidal stiffener had a 10 mm outer height which reduces to 5 mm at a 5 mm depth.

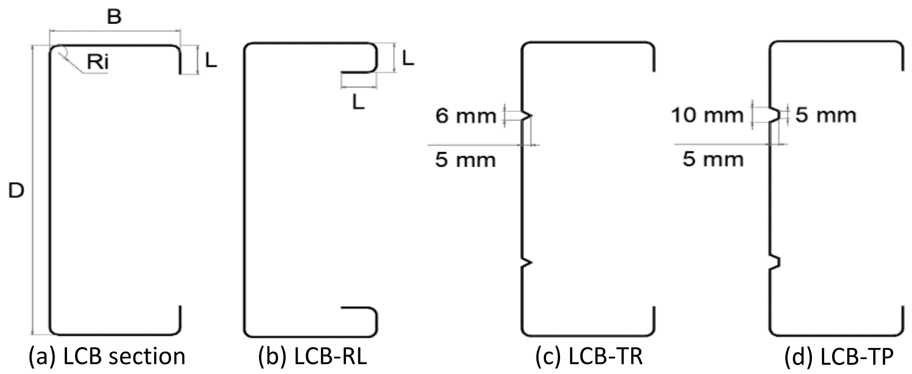

Fig. 4 Cross-section details of LCB section and stiffened sections

Table 2 summarises the different parameters considered to study the shear behaviour of stiffened LCB sections illustrated in Fig. 4. The effect of three different section depths, four different section thicknesses, and four different stainless steel grades was investigated in the parametric study to generate a numerical database. 48 FE models were developed for each section, therefore, generating 144 FE models in total. Then, the gathered numerical results were utilised in understanding the shear behaviour of stainless steel stiffened sections and to evaluate the design rules.

Table 2 Summary of the parameters

Section	Depth, D (mm)	Thickness, t (mm)	Stainless steel grade
LCBs with return lips (LCB-RL) LCBs with triangular web stiffeners (LCB-TR) LCBs with trapezoidal web stiffeners (LCB-TP)	150, 200, 250	1, 1.2, 1.5, 2	Austenitic-1.4301, 1.4311 Duplex-1.4362, 1.4462

4.2 Summary of generated numerical results

The ultimate shear resistances of each section for each stainless steel grade obtained from the numerical parametric study are given in Tables 3-5. When developing the FE models in the parametric study, Young's modulus and Poisson's ratio were taken as 200,000 MPa and 0.3, respectively according to EN1993-1-4 [5]. All the developed sections have an aspect ratio of 1.0 to govern the shear failure.

Table 3 Parametric study results with EN1993-1-4 [5] and the DSM predictions for LCB-RL sections

Section	Stainless steel grade – 1.4301					Stainless steel grade – 1.4311					Stainless steel grade – 1.4362					Stainless steel grade – 1.4462				
	V_{FE}	V_{FE}/V_{EC3}	$V_{FE}/V_{EC3,\text{Proposed}}$	V_{FE}/V_{DSM}	$V_{FE}/V_{DSM,\text{Proposed}}$	V_{FE}	V_{FE}/V_{EC3}	$V_{FE}/V_{EC3,\text{Proposed}}$	V_{FE}/V_{DSM}	$V_{FE}/V_{DSM,\text{Proposed}}$	V_{FE}	V_{FE}/V_{EC3}	$V_{FE}/V_{EC3,\text{Proposed}}$	V_{FE}/V_{DSM}	$V_{FE}/V_{DSM,\text{Proposed}}$	V_{FE}	V_{FE}/V_{EC3}	$V_{FE}/V_{EC3,\text{Proposed}}$	V_{FE}/V_{DSM}	$V_{FE}/V_{DSM,\text{Proposed}}$
LCB-RL 150×65×15×1.0	15.39	1.10	1.01	1.06	1.01	18.32	1.12	1.01	1.09	1.02	24.55	1.11	1.00	1.09	1.01	26.3	1.10	0.99	1.10	1.00
LCB-RL 150×65×15×1.2	20.15	1.09	1.00	1.02	1.00	24.34	1.11	1.02	1.06	1.02	33.45	1.12	1.02	1.09	1.03	36.01	1.12	1.01	1.10	1.03
LCB-RL 150×65×15×1.5	27.73	1.08	1.00	0.98	0.97	33.38	1.09	1.00	1.01	0.99	47.18	1.11	1.02	1.06	1.02	51.02	1.12	1.02	1.07	1.02
LCB-RL 150×65×15×2.0	40.82	1.01	0.96	1.04	1.04	49.78	1.07	0.98	1.01	1.01	70.87	1.08	1.00	0.99	0.98	76.89	1.08	1.00	1.00	0.99
LCB-RL 200×75×20×1.0	17.5	1.12	1.01	1.10	1.02	20.58	1.13	1.01	1.12	1.02	27.2	1.12	0.99	1.12	0.99	28.89	1.11	0.99	1.11	0.98
LCB-RL 200×75×20×1.2	23.67	1.13	1.02	1.09	1.03	28.25	1.14	1.03	1.12	1.04	37.11	1.12	1.00	1.11	1.01	39.46	1.11	0.99	1.11	1.00
LCB-RL 200×75×20×1.5	32.06	1.07	0.98	1.02	0.98	38.78	1.10	1.00	1.06	1.01	53.76	1.12	1.01	1.10	1.02	58.08	1.13	1.02	1.11	1.03
LCB-RL 200×75×20×2.0	48.68	1.06	0.98	0.96	0.96	58.52	1.07	0.99	0.99	0.97	82.25	1.09	0.99	1.04	1.00	89.25	1.09	1.00	1.05	1.00
LCB-RL 250×75×20×1.0	19.02	1.13	1.01	1.12	1.01	22.25	1.14	1.01	1.14	1.00	28.87	1.12	0.99	1.12	0.96	30.5	1.11	0.98	1.11	0.94
LCB-RL 250×75×20×1.2	25.18	1.10	0.99	1.09	1.00	30.15	1.13	1.01	1.12	1.02	39.5	1.11	0.99	1.11	0.98	41.85	1.10	0.98	1.10	0.96
LCB-RL 250×75×20×1.5	35.39	1.08	0.98	1.05	0.99	42.33	1.10	0.99	1.08	1.00	58.52	1.13	1.01	1.12	1.02	62.5	1.12	1.00	1.12	1.01
LCB-RL 250×75×20×2.0	53.38	1.04	0.95	0.97	0.95	64.61	1.06	0.97	1.01	0.97	90.35	1.09	0.98	1.06	0.99	97.79	1.09	0.99	1.07	1.00
Mean		1.08	0.99	1.04	1.00		1.10	1.00	1.07	1.01		1.11	1.00	1.09	1.00		1.11	1.00	1.09	1.00
COV		0.033	0.022	0.052	0.029		0.026	0.018	0.050	0.021		0.014	0.012	0.038	0.020		0.012	0.014	0.032	0.025

Table 4 Parametric study results with EN1993-1-4 [5] and the DSM predictions for LCB-TR sections

Section	Stainless steel grade – 1.4301					Stainless steel grade – 1.4311					Stainless steel grade – 1.4362					Stainless steel grade – 1.4462				
	V_{FE}	V_{FE}/V_{EC3}	$V_{FE}/V_{EC3,Proposed}$	V_{FE}/V_{DSM}	$V_{FE}/V_{DSM,Proposed}$	V_{FE}	V_{FE}/V_{EC3}	$V_{FE}/V_{EC3,Proposed}$	V_{FE}/V_{DSM}	$V_{FE}/V_{DSM,Proposed}$	V_{FE}	V_{FE}/V_{EC3}	$V_{FE}/V_{EC3,Proposed}$	V_{FE}/V_{DSM}	$V_{FE}/V_{DSM,Proposed}$	V_{FE}	V_{FE}/V_{EC3}	$V_{FE}/V_{EC3,Proposed}$	V_{FE}/V_{DSM}	$V_{FE}/V_{DSM,Proposed}$
LCB-TR 150×65×15×1.0	17.04	1.03	1.04	0.95	1.04	20.29	1.04	1.05	0.97	1.05	27.23	1.01	1.04	0.98	1.03	29.06	1.00	1.03	0.97	1.03
LCB-TR 150×65×15×1.2	21.37	1.02	1.01	0.92	1.00	25.74	1.03	1.02	0.95	1.02	34.47	1.00	1.00	0.95	1.00	36.92	0.99	1.00	0.95	1.00
LCB-TR 150×65×15×1.5	28.26	1.01	0.97	0.95	0.95	34.31	1.03	0.99	0.92	0.98	48.21	1.03	1.01	0.96	1.01	52.16	1.03	1.01	0.97	1.01
LCB-TR 150×65×15×2.0	40.80	0.91	1.01	1.04	1.04	49.70	0.99	1.02	1.01	1.01	70.93	1.03	0.97	0.93	0.97	77.52	1.04	0.98	0.95	0.98
LCB-TR 200×75×20×1.0	18.26	0.99	1.00	0.95	1.00	21.28	0.98	1.00	0.95	1.00	27.67	0.94	0.97	0.93	0.96	29.81	0.95	0.98	0.94	0.97
LCB-TR 200×75×20×1.2	24.67	1.04	1.03	0.98	1.03	28.91	1.03	1.03	0.99	1.03	38.43	1.01	1.02	0.99	1.02	41.30	1.01	1.02	0.99	1.02
LCB-TR 200×75×20×1.5	33.35	1.03	1.00	0.96	1.00	40.49	1.05	1.03	0.99	1.03	55.34	1.05	1.03	1.02	1.05	59.31	1.05	1.03	1.02	1.05
LCB-TR 200×75×20×2.0	49.37	1.03	0.97	0.93	0.96	59.73	1.04	0.99	0.95	0.99	84.40	1.06	1.02	1.00	1.03	91.60	1.07	1.02	1.01	1.04
LCB-TR 250×75×20×1.0	19.50	0.98	1.00	0.97	1.00	22.69	0.98	1.00	0.97	1.00	29.76	0.96	1.00	0.96	0.98	31.51	0.95	0.99	0.96	0.97
LCB-TR 250×75×20×1.2	26.24	1.02	1.02	0.99	1.02	30.95	1.02	1.03	1.01	1.03	41.04	1.01	1.03	1.01	1.03	43.67	1.00	1.02	1.00	1.02
LCB-TR 250×75×20×1.5	36.86	1.04	1.01	0.99	1.02	44.02	1.05	1.03	1.02	1.04	59.91	1.06	1.05	1.04	1.06	64.32	1.06	1.05	1.05	1.06
LCB-TR 250×75×20×2.0	54.44	1.02	0.96	0.95	0.97	65.91	1.04	0.99	0.98	1.00	91.46	1.05	1.01	1.02	1.03	99.81	1.06	1.03	1.04	1.05
Mean		1.01	1.00	0.97	1.00		1.02	1.01	0.98	1.01		1.02	1.01	0.98	1.01		1.02	1.01	0.99	1.02
COV		0.035	0.025	0.033	0.029		0.026	0.021	0.029	0.023		0.037	0.023	0.037	0.030		0.040	0.022	0.038	0.031

Table 5 Parametric study results with EN1993-1-4 [5] and the DSM predictions for LCB-TP sections

Section	Stainless steel grade – 1.4301					Stainless steel grade – 1.4311					Stainless steel grade – 1.4362					Stainless steel grade – 1.4462				
	V_{FE}	V_{FE}/V_{EC3}	$V_{FE}/V_{EC3,\ Proposed}$	V_{FE}/V_{DSM}	$V_{FE}/V_{DSM,\ Proposed}$	V_{FE}	V_{FE}/V_{EC3}	$V_{FE}/V_{EC3,\ Proposed}$	V_{FE}/V_{DSM}	$V_{FE}/V_{DSM,\ Proposed}$	V_{FE}	V_{FE}/V_{EC3}	$V_{FE}/V_{EC3,\ Proposed}$	V_{FE}/V_{DSM}	$V_{FE}/V_{DSM,\ Proposed}$	V_{FE}	V_{FE}/V_{EC3}	$V_{FE}/V_{EC3,\ Proposed}$	V_{FE}/V_{DSM}	$V_{FE}/V_{DSM,\ Proposed}$
LCB-TP 150×65×15×1.0	17.25	0.97	1.01	0.87	1.02	20.97	0.99	1.04	0.90	1.04	28.80	0.98	1.04	0.92	1.03	30.52	0.96	1.03	0.91	1.01
LCB-TP 150×65×15×1.2	21.75	0.97	0.99	0.91	0.99	26.43	0.98	1.01	0.88	1.01	37.52	1.00	1.04	0.93	1.03	40.49	0.99	1.04	0.93	1.03
LCB-TP 150×65×15×1.5	29.21	0.92	0.98	0.99	0.99	35.56	0.99	0.98	0.95	0.99	50.83	1.01	1.02	0.92	1.01	55.39	1.02	1.03	0.93	1.02
LCB-TP 150×65×15×2.0	40.98	0.91	0.97	1.05	1.05	49.92	0.89	0.98	1.01	1.01	71.48	0.99	0.96	0.93	0.95	77.95	0.99	0.96	0.91	0.95
LCB-TP 200×75×20×1.0	19.90	0.99	1.04	0.93	1.03	22.84	0.96	1.01	0.92	1.00	29.91	0.92	0.99	0.90	0.97	31.59	0.91	0.97	0.89	0.95
LCB-TP 200×75×20×1.2	25.70	1.00	1.02	0.93	1.02	30.10	0.98	1.02	0.93	1.01	38.99	0.93	0.97	0.90	0.96	41.68	0.92	0.97	0.90	0.96
LCB-TP 200×75×20×1.5	34.79	1.01	1.00	0.92	1.00	41.76	1.01	1.02	0.94	1.01	56.05	0.99	1.00	0.94	1.00	59.93	0.98	0.99	0.94	0.99
LCB-TP 200×75×20×2.0	50.17	1.01	0.96	0.95	0.95	61.19	1.02	0.99	0.92	0.98	85.31	1.02	1.00	0.95	1.00	92.57	1.03	1.00	0.96	1.01
LCB-TP 250×75×20×1.0	19.95	0.92	0.97	0.89	0.95	22.57	0.89	0.94	0.87	0.92	29.32	0.86	0.92	0.85	0.89	31.25	0.85	0.92	0.85	0.89
LCB-TP 250×75×20×1.2	27.71	0.99	1.02	0.95	1.01	31.95	0.97	1.00	0.94	0.99	41.54	0.93	0.98	0.92	0.96	44.28	0.93	0.97	0.92	0.96
LCB-TP 250×75×20×1.5	37.57	0.99	0.99	0.93	0.99	44.32	0.99	0.99	0.95	0.99	59.87	0.98	1.00	0.96	1.00	63.16	0.96	0.98	0.94	0.98
LCB-TP 250×75×20×2.0	55.68	1.00	0.96	0.92	0.96	66.93	1.01	0.98	0.94	0.98	94.00	1.03	1.01	0.99	1.02	101.60	1.03	1.02	1.00	1.03
Mean		0.97	0.99	0.94	0.99		0.97	1.00	0.93	0.99		0.97	0.99	0.93	0.98		0.96	0.99	0.92	0.98
COV		0.037	0.026	0.048	0.030		0.045	0.026	0.039	0.028		0.052	0.034	0.036	0.041		0.056	0.035	0.040	0.043

5 FE modelling of elastic shear buckling behaviour

5.1 General

In general, the design of steel sections for shear is associated with the calculation of elastic shear buckling stresses. European standards for the design of stainless steel, EN1993-1-4 [5] adopt the equations given in European standards for plated steel, EN1993-1-5 [6] for the calculation of shear buckling coefficients of constituent plate elements of a section. In addition, European standards for cold-formed steel, EN1993-1-3 [29] employs separate provisions for the shear buckling coefficient calculation which usually deals with cumbersome calculations, in particular when intermediate stiffeners are present.

Alternatively, the DSM considers the buckling of whole cross-sections in the shear buckling coefficient calculation. Therefore, the aid of numerical tools is sought when determining the solutions for the shear buckling of thin-walled sections in the DSM. The use of FSM and FEM is more common in achieving this. The shear buckling of cold-formed channel sections with plain webs has been investigated by Pham and Hancock [30] while that for sections with both plain and longitudinally stiffened webs has been studied by Pham et al. [4] and Hancock and Pham [31] using FSM. Further, Keerthan and Mahendran [32], [33] incorporated FEM in determining the shear buckling characteristics of cold-formed sections including LCBs. In this study, FEM was utilised to investigate the elastic shear buckling response of the considered cold-formed LCB cross-sections with stiffeners.

5.2 FE model development

The details of FE modelling carried out to investigate the elastic shear buckling behaviour of cold-formed stainless steel channel sections with stiffeners are briefed in this section. Abaqus software was utilised for this purpose.

In the FE modelling conducted to study the shear buckling behaviour, the channel sections were simulated without any transverse stiffeners or flange restraints as opposed to the shear FE models described in Section 2. A mid-span load was applied to the simply supported sections with an aspect ratio of 1.0 to simulate the shear buckling behaviour. Four node quadrilateral S4R shell elements with six DOFs at each node were employed to model the shear buckling behaviour of thin steel sections. As described in Section 2.1, a 5 mm × 5 mm mesh was assigned to the flat parts and a relatively finer mesh of 1 mm × 5 mm was employed to the corner regions of the sections. Modified two-stage Ramberg-Osgood material model [24] was adopted here as well to represent stainless steel behaviour under shear buckling. Young's modulus was taken as 200,000 MPa and a value of 0.3 was used for Poisson's ratio.

Boundary conditions were chosen appropriately. Pin and roller support conditions were maintained at the two section ends to simulate the simply supported conditions. For this, in-plane translations were restrained in the cross-sectional plane (x-y plane) at both ends and out-of-plane translations (in the z-direction) of the cross-sectional plane was restrained at the left end. Further, rotation about the longitudinal axis (z-axis) of the section was fixed at both ends to suppress torsional effects. At the mid-span of the section, translations in the x-z plane and rotation about the z-axis were restrained to provide roller support conditions to the loading plane. All these restraints were assigned to the entire cross-sections including webs, flanges and lips to take into account the effect of the shear flow of the full cross-section to the shear buckling. To generate shear buckling behaviour in the sections, a 1 kN force was applied to the section web at the mid-span. Fig. 5 illustrates the assigned boundary conditions in the FE models to study the shear buckling behaviour of LCB sections.

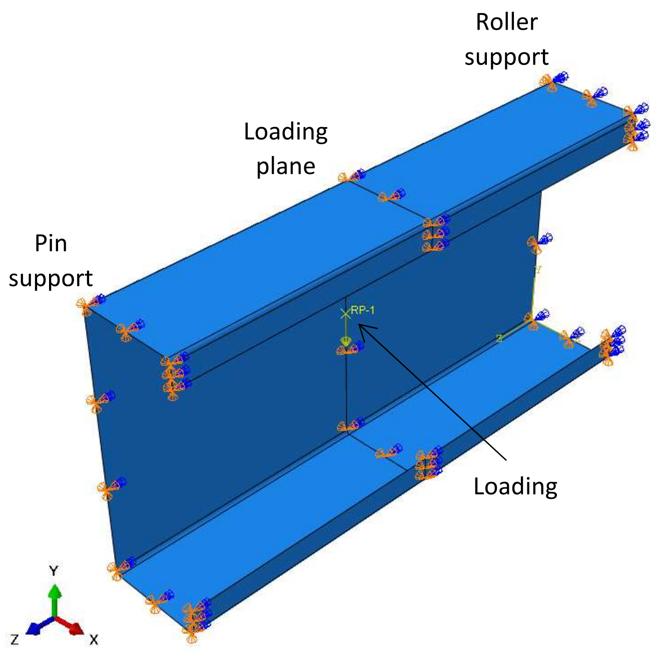

Fig. 5 Boundary conditions assigned to LCBs in the shear buckling analysis

Then, an Eigenvalue buckling analysis was performed on each section. From the results, Eigenmodes and corresponding Eigenvalues were extracted. The Eigenmodes represent the elastic shear buckling behaviour of the section and corresponding Eigenvalues provide the shear buckling force of the respective mode. The critical elastic shear buckling modes and corresponding shear buckling forces were identified for each varying cross-section considered in the study. Usually, the lowest values are taken as critical.

5.3 Calculation of shear buckling coefficients

Timoshenko and Gere [34] investigated the shear buckling behaviour of flat rectangular plates and derived an equation to calculate the elastic shear buckling stress (τ_{cr}) of a thin plate. When the plate is simply supported at its four edges and is subjected to shear stresses, out-of-plane buckling stress is given by Eq. (4) according to Timoshenko and Gere [34].

$$\tau_{cr} = \frac{k_{\upsilon}\pi^2 E}{12\,(1-\upsilon^2)}\left(\frac{t}{d_1}\right)^2 \tag{4}$$

where E is Young's modulus, υ is Poisson's ratio, t is plate thickness and d_1 is plate height. k_v is the shear buckling coefficient of the plate which depends on the aspect ratio of the plate and the edge conditions of the plate. The shear buckling coefficient of a simply supported plate varies from 5.34 for a very lengthy plate to 9.34 for a square plate.

Eq. (4) can be applied to cross-section webs if the corresponding shear buckling coefficient of the section is known. Unlike the simply supported plates, the presence of flanges at the top and bottom edges enhances the shear buckling resistance of the cross-section webs. The intermediate web stiffeners further increase the buckling resistance. The use of numerical tools allows taking into account the behaviour of full cross-sections including the flanges to the shear buckling of section webs. The effect of intermediate web stiffeners can also be treated in the analysis. The shear buckling force (V_{cr}) of a section web can be related to the shear buckling stress given in Eq. (4) using the cross-sectional area of the web. Therefore, the shear buckling coefficient can be back-calculated from Eq. (4) if the shear buckling force of the section web is known from the numerical analysis.

Keerthan and Mahendran [30] proposed an equation for the calculation of the shear buckling coefficients of cold-formed sections using FE results and is expressed by Eq. (5).

$$k_{\upsilon} = k_{ss} + n(k_{sf} - k_{ss}) \tag{5}$$

where k_{ss} and k_{sf} are the shear buckling coefficients of the web plates with simple-simple and simple-fixed end conditions, respectively. The coefficient 'n' accounts for the level of fixity at the web to flange junction which depends on the geometry of the cold-formed section. A value of n=0.23 was suggested for LCBs by Keerthan and Mahendran [29]. Therefore, the shear buckling coefficient of LCB sections with an aspect ratio of 1.0 is equal to a value of 10.09 according to Eq (5).

From the elastic shear buckling analysis conducted in Section 5.2, Eigenvalues were extracted for each section considered and these were incorporated in back-calculating the shear buckling coefficient of each section. First, the calculated shear buckling coefficients of LCBs were compared with Eq. (5) to confirm the accuracy of the numerical model to predict the shear buckling force of the section. Table 6 summarises all the numerical results generated in the shear buckling analysis, the back-calculated shear buckling coefficients for each section and the comparison of shear buckling coefficients of each section with the shear buckling coefficient of LCB sections calculated from Eq. (5). From the comparison, it can be seen that the ratio between the back-calculated coefficient and the coefficient derived from Eq. (5) for LCBs has a mean and a COV of 0.99 and 0.006, respectively. Therefore, it can be concluded that the numerical analysis is able to predict the shear buckling forces of the sections with good accuracy.

Further, Fig. 6 plots the shear buckling coefficients of each section considered. It is seen from Fig. 6 that LCB sections with return lips have shear buckling coefficients which are almost equal to that of LCB sections. The ratio between the back-calculated shear buckling coefficient of the sections with return lips and the shear buckling coefficient derived from Eq. (5) for LCBs further confirm this with a mean of 1.00 and a COV of 0.006. According to Fig. 6, LCB sections with triangular and trapezoidal web stiffeners exhibits higher shear buckling coefficients compared to LCB sections. The sections with trapezoidal web stiffeners feature the highest coefficients among the considered sections. The variation of the magnitude of the shear buckling coefficients of web stiffened sections is associated with the variation of the web stiffener indent. Therefore, it can be concluded that the web stiffeners enhance the shear buckling resistance of the sections. Further, it is seen that the higher the indent of the web stiffener is, the higher the shear buckling coefficient.

Table 6 Elastic shear buckling analysis results

No.	Section	LCB			LCB-RL			LCB-TR			LCB-TP		
		$V_{cr,FE}$ (kN)	$k_{v,FE}$	$k_{v,FE}$/ $k_{LCB,Eq.(5)}$	$V_{cr,FE}$ (kN)	$k_{v,FE}$	$k_{v,FE}$/ $k_{LCB,Eq.(5)}$	$V_{cr,FE}$ (kN)	$k_{v,FE}$	$k_{v,FE}$/ $k_{LCB,Eq.(5)}$	$V_{cr,FE}$ (kN)	$k_{v,FE}$	$k_{v,FE}$/ $k_{LCB,Eq.(5)}$
1	Section 150×65×15×1.0	12.61	10.047	1.00	12.72	10.133	1.00	23.51	18.731	1.86	32.53	25.912	2.57
2	Section 150×65×15×1.2	21.80	10.021	0.99	21.98	10.105	1.00	36.13	16.610	1.65	50.15	23.053	2.28
3	Section 150×65×15×1.5	42.57	9.979	0.99	42.92	10.061	1.00	61.42	14.396	1.43	83.35	19.536	1.94
4	Section 150×65×15×2.0	100.92	9.909	0.98	101.69	9.985	0.99	125.09	12.283	1.22	157.26	15.442	1.53
5	Section 200×75×20×1.0	9.35	10.035	0.99	9.44	10.131	1.00	16.16	17.347	1.72	21.96	23.571	2.34
6	Section 200×75×20×1.2	16.16	10.017	0.99	16.32	10.112	1.00	25.04	15.523	1.54	33.85	20.982	2.08
7	Section 200×75×20×1.5	31.57	9.988	0.99	31.87	10.082	1.00	43.25	13.682	1.36	56.57	17.895	1.77
8	Section 200×75×20×2.0	74.87	9.940	0.99	75.55	10.031	0.99	90.23	11.979	1.19	109.12	14.487	1.44
9	Section 250×75×20×1.0	7.37	9.946	0.99	7.45	10.053	1.00	12.05	16.268	1.61	16.15	21.801	2.16
10	Section 250×75×20×1.2	12.74	9.932	0.98	12.87	10.036	0.99	18.82	14.680	1.45	24.89	19.411	1.92
11	Section 250×75×20×1.5	24.88	9.908	0.98	25.13	10.009	0.99	32.92	13.112	1.30	41.82	16.658	1.65
12	Section 250×75×20×2.0	58.98	9.870	0.98	59.53	9.962	0.99	69.81	11.683	1.16	82.14	13.746	1.36
	Mean		9.966	0.99		10.058	1.00						
	COV		0.006	0.006		0.006	0.006						

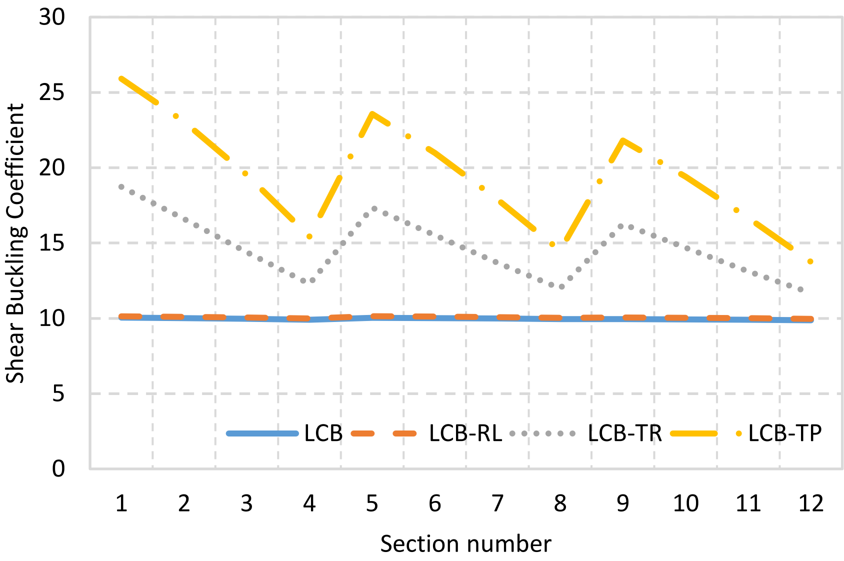

Fig. 6 Comparison of shear buckling coefficients of different sections

5.4 Shear buckling modes

Fig. 7 illustrates the identified critical elastic shear buckling modes of each section. From Figs. 7 (a) and (b), it can be seen that both plain LCBs and LCBs with return lips have similar shear buckling modes with single buckling half-waves. Further, it can be observed that the shear buckling modes of LCBs with triangular and trapezoidal web stiffeners are similar to each other from Figs. 7 (c) and (d). However, LCB sections with longitudinal web stiffeners exhibit two buckling half-waves. Therefore, it can be concluded that the presence of longitudinal web stiffeners reduces the length of buckling half-waves of the section. However, the shape of the stiffener does not have any significant effect on the buckling half-wave length of the section as observed from Fig. 7. Moreover, the spreading of the buckling mode over the whole web and the buckling of the web stiffeners can be observed in web stiffened LCB sections.

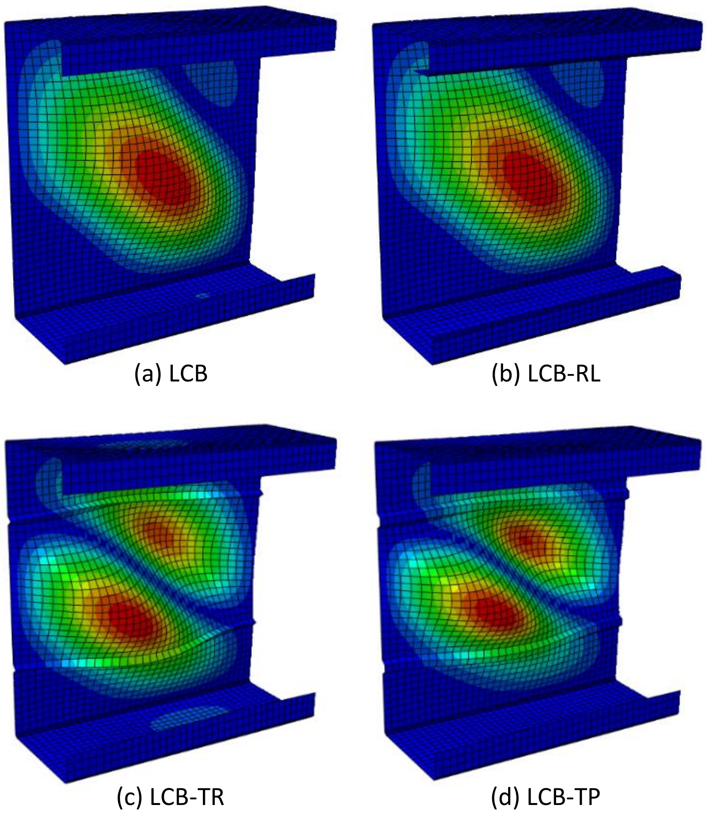

Fig. 7 Elastic shear buckling modes of different cross-sections

6 Analysis of FE shear failure modes

The structural behaviour of the cold-formed stainless steel stiffened channel sections subjected to shear was investigated in this section using numerical results generated in the parametric study. The failure mechanism of each different section type was observed at different stages of the load-deflection curve. Figs. 8-10 illustrate the failure mechanisms of each section type investigated in this study alongside their load-deflection curves. From Fig. 8, it can be observed that the shear buckling of both webs of LCB-RL 200×75×20×1.0 section with return lips. The out-of-plane buckling of webs was approximately started at Point 1 of the load-deflection curve and the progression of the web buckling was observed when the section reaches the post-peak loading region.

Figs. 9 and 10 depict the web shear buckling of channel sections with triangular and trapezoidal web stiffeners. The buckling of the web stiffener above the neutral axis can be observed for both sections with triangular and trapezoidal stiffeners as a result of compressive stresses in the sections. This is because the stiffness of the web stiffeners is not large enough to resist the out-of-plane buckling induced by the compressive stresses. A shift of the buckling pattern towards the top half of the section webs can be seen with the presence of a web stiffener below the neutral axis. The web stiffener below the neutral axis was able to minimise the out-of-plane buckling of the webs at the post-buckling region with the aid of tensile stresses developed in the section.

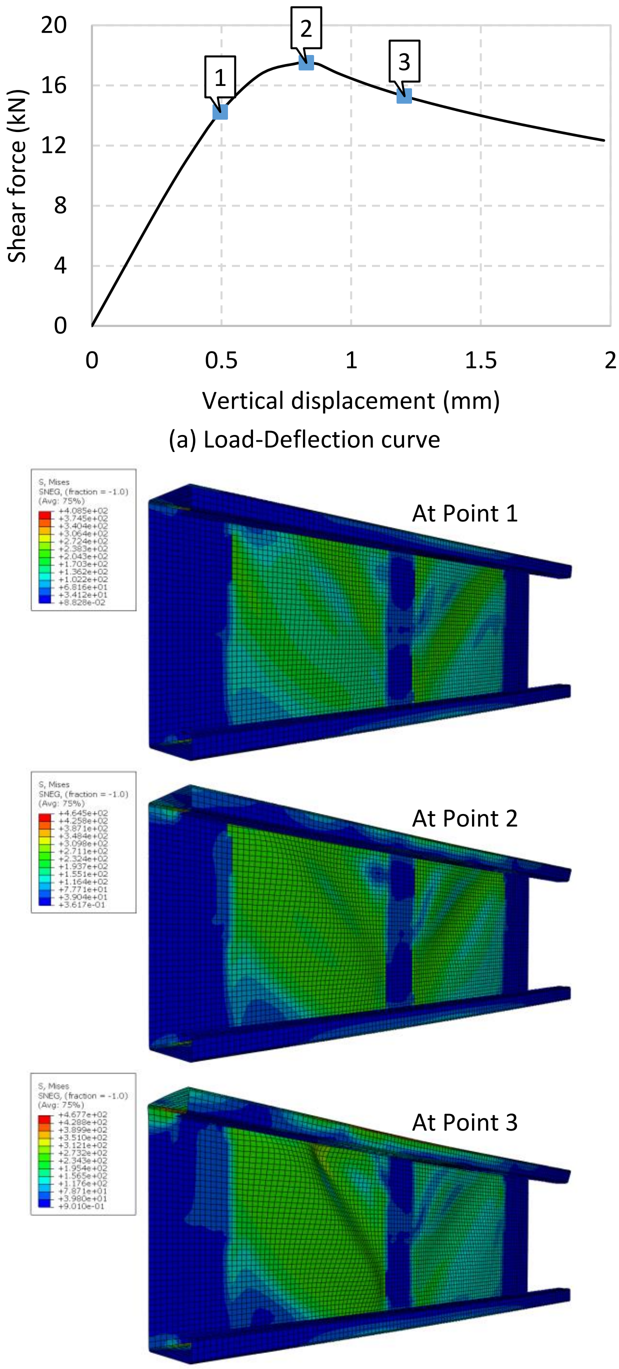

(b) FE shear failure modes

Fig. 8 FE shear failure modes of LCB-RL 200×75×20×1.0 section at the different stages of the load-deflection curve

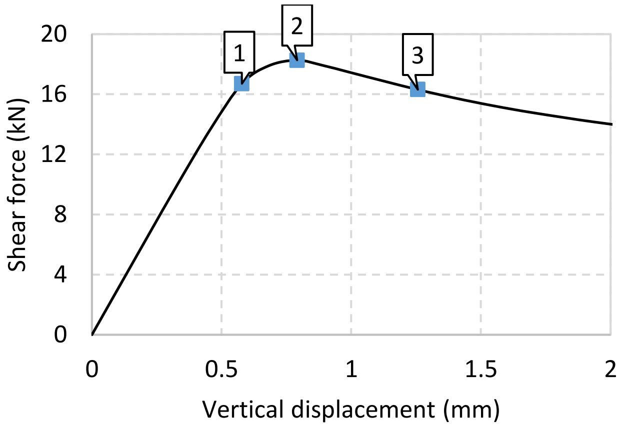

(a) Load-Deflection curve

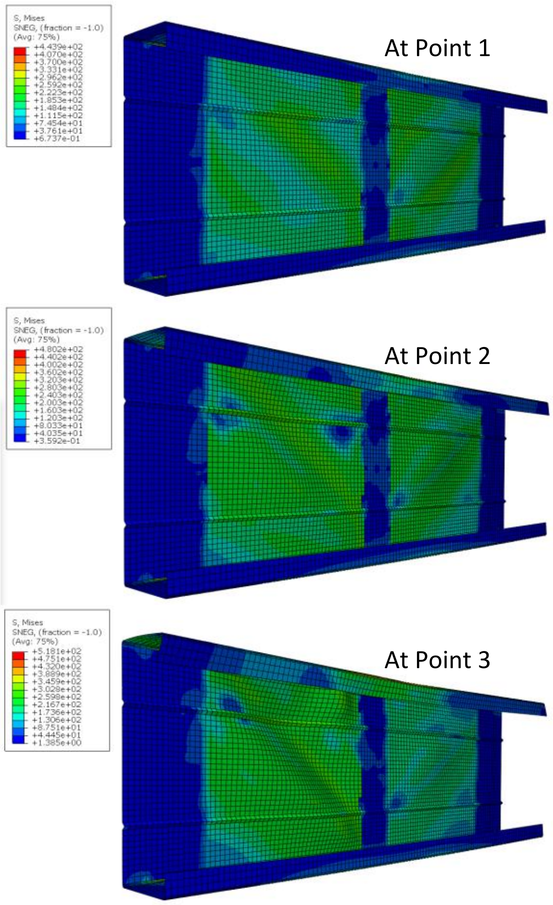

(b) FE shear failure modes

Fig. 9 FE shear failure modes of LCB-TR 200×75×20×1.0 section at the different stages of the load-deflection curve

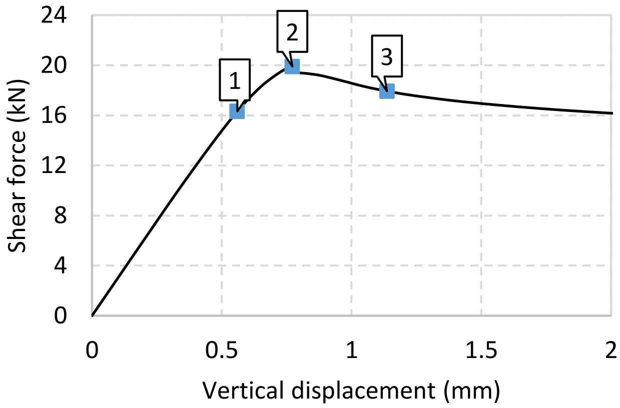

(a) Load-Deflection curve

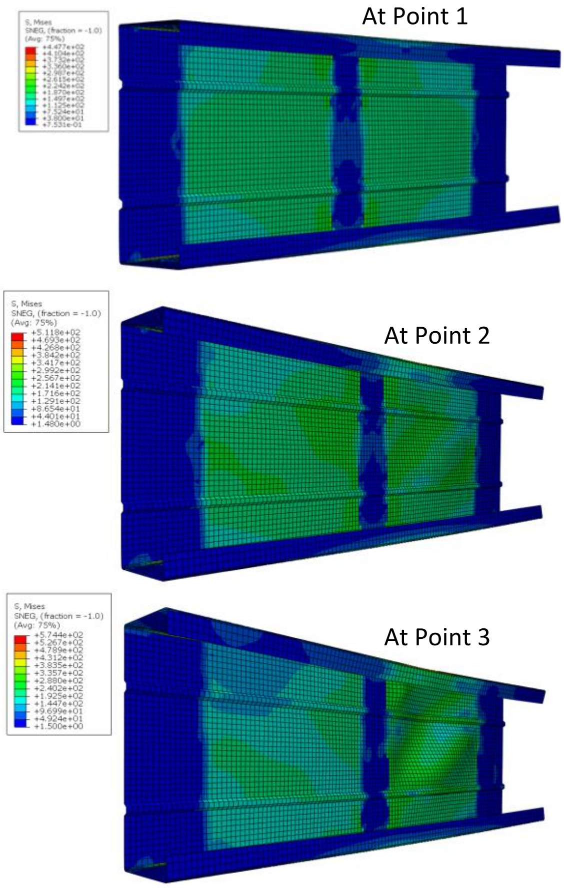

(b) FE shear failure modes

Fig. 10 FE shear failure modes of LCB-TP 200×75×20×1.0 section at the different stages of the load-deflection curve

7 Evaluation of shear design provisions

This section covers the evaluation of EN1993-1-4 [5] and the DSM shear design provisions for cold-formed stainless steel channel sections with stiffeners investigated in the parametric study. The generated numerical results were compared with the code predictions, and modifications were applied to the codified rules where necessary to enhance the resistance prediction accuracy.

7.1 EN1993-1-4 shear design provisions

The shear design provisions provided in European standards for stainless steel, EN1993-1-4 [5] refer to the shear design equations set out in EN1993-1-5 [6] which are based on the rotated stress field method. In EN1993-1-5 [6], the shear resistance ($V_{b,Rd}$) of a section is defined as the summation of the web shear buckling resistance ($V_{bw,Rd}$) and the flange contribution to the shear resistance ($V_{bf,Rd}$). This is expressed in Eq. (6).

$$V_{b,Rd} = V_{bw,Rd} + V_{bf,Rd} \leq \frac{\eta f_{yw} h_w t_w}{\sqrt{3}\gamma_{M1}} \tag{6}$$

where f_{yw} is the yield strength of the web, h_w is the web depth, t_w is the web thickness and γ_{M1} is the partial safety factor. The parameter 'η' takes into account the strain hardening of stainless steel.

The web shear buckling resistance, $V_{bw,Rd}$ is defined by Eq. (7).

$$V_{bw,Rd} = \frac{\chi_w f_{yw} h_w t_w}{\sqrt{3}\gamma_{M1}} \tag{7}$$

where χ_w is the web shear buckling reduction factor.

In EN1993-1-4 [5], separate expressions are provided for web shear buckling reduction factor, χ_w as a function of the web slenderness, $\bar{\lambda}_w$ and these expressions for web panels with rigid end post are given by Eqs. (8)-(10).

$$\chi_w = \eta \text{ for } \bar{\lambda}_w \leq 0.65/\eta \tag{8}$$

$$\chi_w = 0.65/\bar{\lambda}_w \text{ for } 0.65/\eta < \bar{\lambda}_w < 0.65 \tag{9}$$

$$\chi_w = 1.56/(0.91 + \bar{\lambda}_w) \text{ for } \bar{\lambda}_w \geq 0.65 \tag{10}$$

In EN1993-1-5 [6], Eq. (11) is used for the calculation of slenderness ($\bar{\lambda}_w$) of the webs with both transverse stiffeners and longitudinal stiffeners.

$$\bar{\lambda}_w = \frac{h_w}{37.4 t_w \varepsilon \sqrt{k_\tau}} \tag{11}$$

where ε is the material factor and k_τ is the web shear buckling coefficient.

The flange contribution to the section shear resistance, $V_{bf,Rd}$ is given by Eq. (12) which is applied only when the design bending moment (M_{Ed}) of the section is less than the bending resistance of the flanges alone ($M_{f,Rd}$).

$$V_{bf,Rd} = \frac{b_f t_f^2 f_{yf}}{c\,\gamma_{M1}}\left(1 - \left(\frac{M_{Ed}}{M_{f,Rd}}\right)^2\right) \qquad (12)$$

where b_f is the flange width, t_f is the flange thickness and f_{yf} is the yield stress of the flange.

The distance along the flange from the transverse stiffener to the location of the plastic hinge is expressed by the parameter 'c'. An alternative expression for 'c' is defined in EN1993-1-4 [5] and given in Eq. (13).

$$c = a\left[0.17 + \frac{3.5\, b_f t_f^2 f_{yf}}{t_w h_w^2 f_{yw}}\right] \text{ and } \frac{c}{a} \leq 0.65 \qquad (13)$$

where a is the spacing between transverse stiffeners.

Then, numerical shear capacities for cold-formed LCB sections with stiffeners were compared with EN1993-1-4 [5] predictions. For the calculation of EN1993-1-4 [5] shear capacities, the back-calculated shear buckling coefficients found from the numerical shear buckling analysis conducted in Section 5 were incorporated. Tables 3-5 summarise the ratio between the FE shear capacity and EN1993-1-4 [5] predicted shear capacity of each section for each stainless steel grade while Table 7 compares the overall mean and COV values for each section type. From the comparison, it was found that the FE shear capacity to EN1993-1-4 [5] predicted shear capacity ratio for LCBs with return lips have a mean and a COV of 1.10 and 0.024, respectively. Further, the mean and the COV of the FE shear capacity to the predicted shear capacity ratio for LCBs with triangular web stiffeners are 1.02 and 0.034, respectively while those values for LCBs with trapezoidal web stiffeners are 0.97 and 0.047, respectively.

Table 7 Overall mean and COV values of FE to predicted resistance ratio for each section type

	LCB-RL Current	Proposed	LCB-TR Current	Proposed	LCB-TP Current	Proposed
	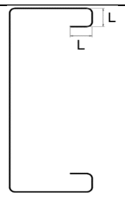		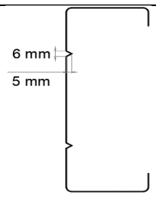		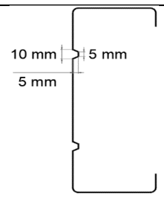	
EN1993-1-4 [5]						
Mean	1.10	1.00	1.02	1.01	0.97	0.99
COV	0.024	0.014	0.034	0.022	0.047	0.035
DSM						
Mean	1.07	1.00	0.98	1.02	0.93	0.98
COV	0.045	0.025	0.034	0.031	0.040	0.043

Fig. 11 compares the FE shear capacities with EN1993-1-4 [5] web shear buckling reduction factor (χ_w) curve for all three section types. The comparison of FE shear capacities with the code predictions suggests that EN1993-1-4 [5] shear provisions are conservative for the cold-formed stainless steel LCB sections with return lips. Further, EN1993-1-4 [5] shear design rules are found to be satisfactory for the LCB sections with triangular web stiffeners, however, it is concluded from the comparisons that the shear capacities of LCB sections with trapezoidal web stiffeners are over-predicted.

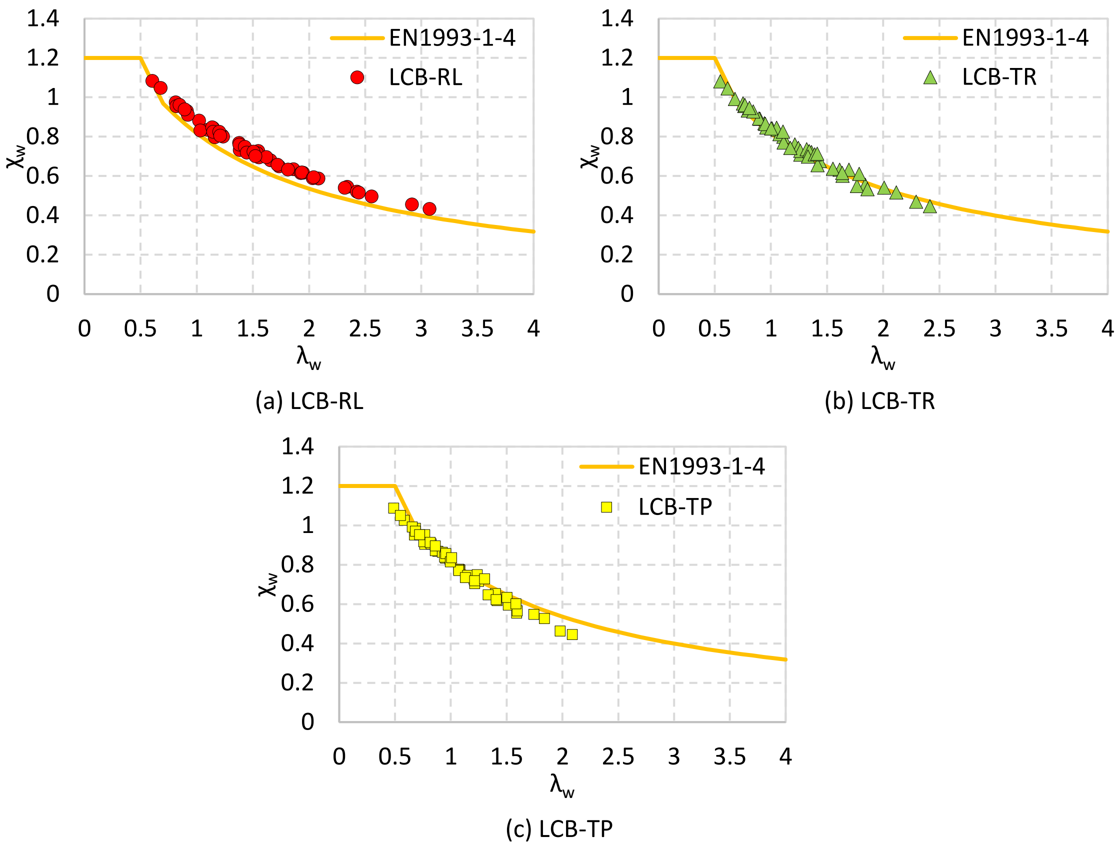

Fig. 11 Comparison of FE shear capacities with EN1993-1-4 [5] curve for web shear buckling reduction factor, χ_w

Dissanayake et al. [13] conducted numerical studies on the shear behaviour of cold-formed stainless steel LCB sections and proposed new design equations. In Fig. 12, the FE results of shear capacities generated for all three section types are compared with the experimental and FE shear capacities of cold-formed stainless steel LCB sections found from Dissanayake et al. [13]. It can be seen that there is no significant enhancement in the shear resistance of cold-formed stainless steel LCB sections with stiffeners considered in this study compared to plain LCB sections. In addition, FE data points shifted along the x-axis with the reduced web slenderness ($\bar{\lambda}_w$) as a result of the higher shear buckling coefficient (k_v) of the sections with web stiffeners.

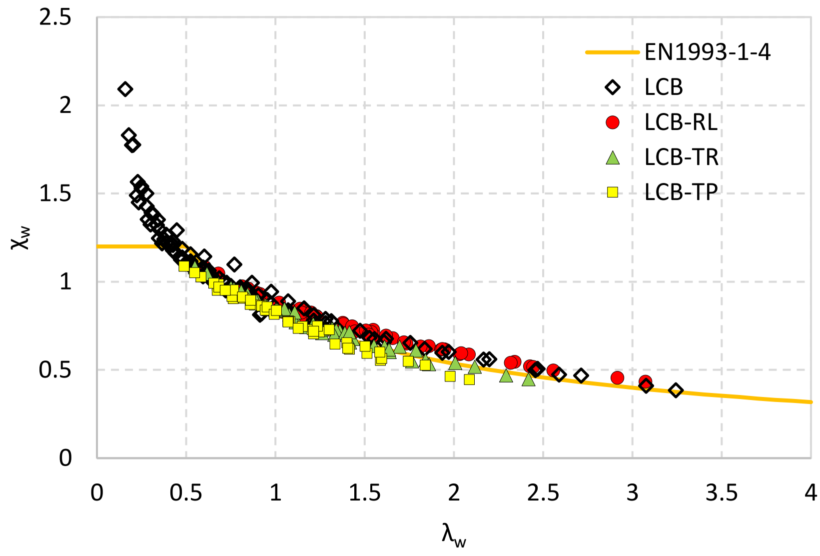

Fig. 12 Comparison of FE shear capacities of stainless steel stiffened LCBs with the experimental and FE shear capacities of plain LCBs found from Dissanayake et al. [13]

Following the evaluation of EN1993-1-4 [5] shear design provisions in predicting the shear resistance of cold-formed stainless steel LCB sections with longitudinal stiffeners, modifications were proposed to EN1993-1-4 [5] web shear buckling reduction factor (χ_w) to enhance the prediction accuracy. For this, web shear buckling resistance ($V_{bw,Rd}$) defined by Eq. (7) was directly compared with the FE shear capacities as the flange contribution ($V_{bf,Rd}$) to the shear resistance of the section given by Eq. (12) was negligible. Two separate sets of expressions were proposed for the web shear buckling reduction factor (χ_w) after following regression analyses. The slenderness limits were defined accordingly in each case at the yield load of the sections.

The proposed expressions for LCB sections with return lips are given by Eqs. (14)-(16).

$$\chi_w = \eta \text{ for } \bar{\lambda}_w \leq 0.65/\eta \quad (14)$$

$$\chi_w = 0.874/\bar{\lambda}_w^{\,0.517} \text{ for } 0.65/\eta < \bar{\lambda}_w < 0.77 \quad (15)$$

$$\chi_w = 1.84/(1.07 + \bar{\lambda}_w) \text{ for } \bar{\lambda}_w \geq 0.77 \quad (16)$$

Then, another set of equations was proposed for LCB section with web stiffeners and is given by Eqs. (17)-(19). In addition to web slenderness ($\bar{\lambda}_w$), these proposed expressions depend on the shear buckling coefficients (k_v) of the sections as well.

$$\chi_w = \eta \text{ for } \bar{\lambda}_w \leq 0.4 \quad (17)$$

$$\chi_w = 0.868/\bar{\lambda}_w^{\,0.353} \text{ for } 0.4 < \bar{\lambda}_w < 0.67 \quad (18)$$

$$\chi_w = 1.52/\left[(0.73 + \bar{\lambda}_w)(k_v/10.09)^{0.14}\right] \text{ for } \bar{\lambda}_w \geq 0.67 \quad (19)$$

Figs. 13 and 14 compare the proposed curves for web shear buckling reduction factor with the FE shear capacities of corresponding LCB sections. The average curve is plotted in Fig. 14 since Eq. (19) is a function of the shear buckling coefficient of each section. It can be seen that proposed curves agree well with the distribution of the FE data points. The FE shear capacity to the predicted shear capacity ratio of each section of each steel grade is listed for each set of proposed expressions in Tables 3-5. From the calculation, it was found that the mean and the COV of the FE shear capacity to the predicted shear capacity ratio are 1.00 and 0.014, respectively for Eqs. (14)-(16) while the FE shear capacity to the predicted shear capacity ratio has a mean and a COV of 1.00 and 0.028, respectively for Eqs. (17)-(19). Therefore, it can be concluded that proposed expressions for EN1993-1-4 [5] web shear buckling reduction factor (χ_w) are able to accurately predict the shear resistance of the considered LCB sections with stiffeners and provide increased accuracy over the codified expressions.

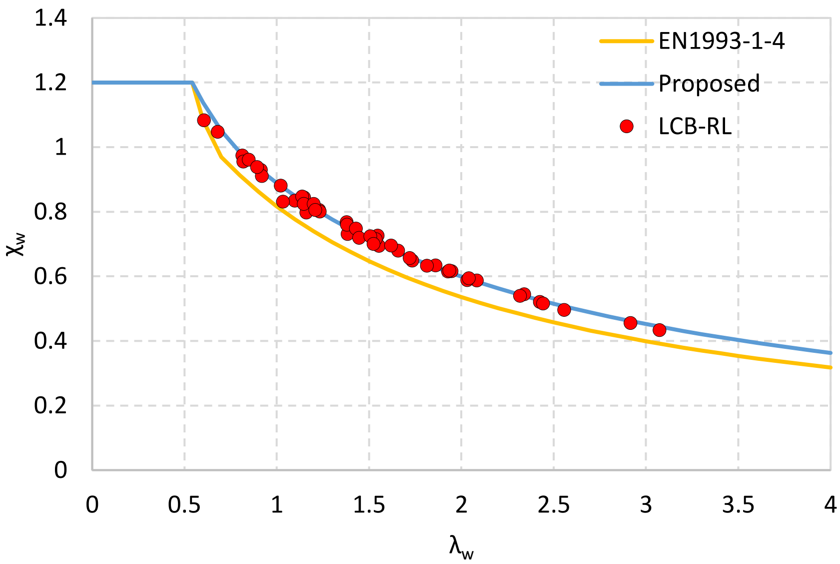

Fig. 13 Comparison of FE shear capacities of LCB-RL sections with the proposed curve for EN1993-1-4 [5] web shear buckling reduction factor, χ_w

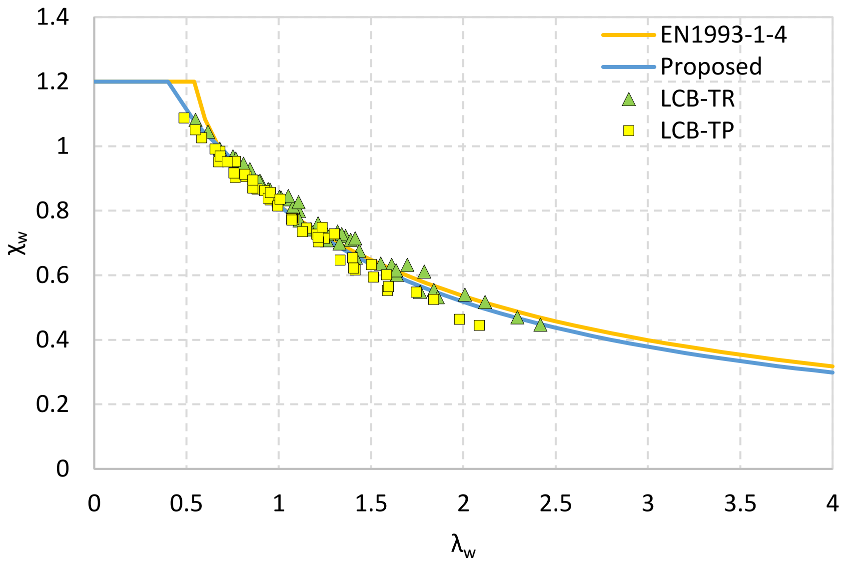

Fig. 14 Comparison of FE shear capacities of LCB-TR and LCB-TP sections with the proposed curve for EN1993-1-4 [5] web shear buckling reduction factor, χ_w

7.2 The DSM shear design provisions

In the DSM, all the elastic instabilities of the gross cross-section are taken into account to determine the section strength. The DSM shear design provisions for the sections with transverse web stiffeners are provided in the clause 7.2.3.3 of AS/NZS 4600 [11]. Eqs. (20) and (21) defines the shear strength (V_v) of a section according to the DSM.

$$V_v = V_y \text{ for } \lambda \leq 0.776 \tag{20}$$

$$V_v = \left[1 - 0.15\left(\frac{1}{\lambda^2}\right)^{0.4}\right]\left(\frac{1}{\lambda^2}\right)^{0.4} V_y \text{ for } \lambda > 0.776 \tag{21}$$

where λ is the slenderness of the cross-section.

The slenderness (λ) of the section can be calculated from Eq. (22) by determining the yield strength (V_y) and the elastic shear buckling strength (V_{cr}) of the section.

$$\lambda = \sqrt{\frac{V_y}{V_{cr}}} \tag{22}$$

The yield strength (V_y) of the section is given by Eq. (23).

$$V_y = 0.6\, f_{yw} d_1 t_w \tag{23}$$

where d_1 is the flat depth of the web.

For the calculation of the elastic shear buckling strength (V_{cr}), Eq. (4) given in Section 5.3 can be used. Further, numerical analysis can also be conducted to find out the elastic shear buckling strength as described previously in Section 5.

Then, the DSM shear design provisions were compared with the FE shear capacities of cold-formed stainless steel LCB sections with stiffeners in this section. For the calculation of DSM shear capacities, back-calculated shear buckling coefficients were utilised from Section 5. The ratio between the FE shear capacity and the predicted shear capacity from the DSM of each section for each steel grade studied is given in Tables 3-5. The overall mean and COV values for each section type are compared in Table 7. The mean and the COV of the FE shear capacity to the DSM shear capacity ratio of LCB sections with return lips are found to be 1.07 and 0.045, respectively. Further, the FE shear capacity to the DSM shear capacity ratio for LCBs with triangular stiffeners has a mean and a COV of 0.98 and 0.034, respectively while that of LCBs with trapezoidal stiffeners are 0.93 and 0.040, respectively.

Fig. 15 illustrates the FE shear capacities of each LCB section type analysed with the DSM shear design curve. It can be concluded from all these comparisons of FE shear capacities with the DSM predictions that the DSM shear design rules are conservative for cold-formed stainless steel LCB sections with return lips while the DSM shear design provisions over-predict the shear capacities of LCB sections with longitudinal web stiffeners studied.

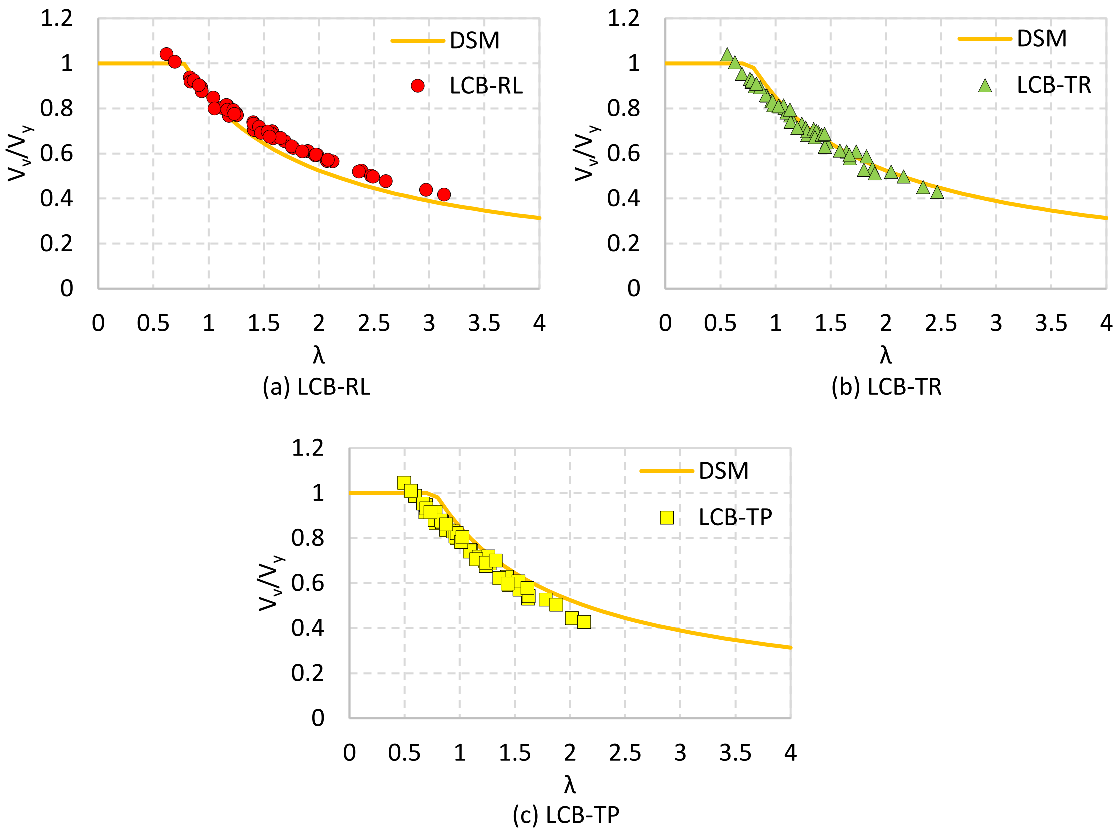

Fig. 15 Comparison of FE shear capacities with the DSM shear design curve

The modified DSM equations were also proposed to enhance the shear capacity prediction accuracy of the cold-formed stainless steel LCB sections with stiffeners using FE results. After conducting regression analyses to fit the distribution of FE data points, two sets of equations were proposed by modifying Eqs. (20) and (21).

Eqs. (24) and (25) give the proposed DSM equations for LCB sections with return lips.

$$V_v = V_y \text{ for } \lambda \leq 0.776 \tag{24}$$

$$V_v = \left[1 - 0.13\left(\frac{1}{\lambda^2}\right)^{0.33}\right]\left(\frac{1}{\lambda^2}\right)^{0.33} V_y \text{ for } \lambda > 0.776 \tag{25}$$

Considering the FE results of LCB sections with web stiffeners, Eqs. (26) and (27) were proposed to predict their shear capacities. Similar to the proposed EN1993-1-4 [5] expression for the web shear buckling reduction factor of web stiffened LCB sections given by Eq. (19), the proposed DSM equation expressed in Eq. (27) is also a function of both slenderness (λ) and shear buckling coefficient (k_v) of the section.

$$V_v = V_y \text{ for } \lambda \leq 0.66 \tag{26}$$

$$V_v = \left[1 - 0.16\left(\frac{k_v}{10.09}\right)^{0.45}\left(\frac{1}{\lambda^2}\right)^{0.395}\right]\left(\frac{1}{\lambda^2}\right)^{0.395} V_y \text{ for } \lambda > 0.66 \quad (27)$$

The proposed DSM equations were compared with the FE shear capacities of the respective sections in Figs. 16 and 17. The average curve for Eq. (27) is plotted in Fig. 17, because Eq. (27) includes the shear buckling coefficient of the section. The comparison of the proposed DSM curves agrees well with the distribution of the FE data points. Further, the FE shear capacity to the predicted shear capacity ratios are given in Tables 3-5 for the proposed DSM equations. It was calculated that the mean and the COV of the FE shear capacity to the predicted shear capacity ratio are 1.00 and 0.025, respectively for Eqs. (24) and (25) while that of Eqs. (26) and (27) are 1.00 and 0.034, respectively. Therefore, the proposed DSM equations provide better shear capacity predictions with increased accuracy compared to the DSM shear design equations given in Eqs. (20) and (21).

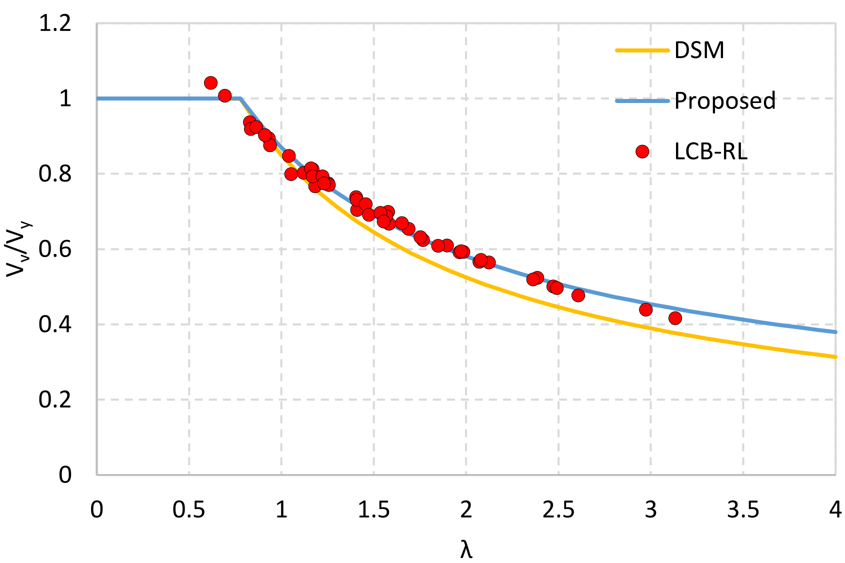

Fig. 16 Comparison of FE shear capacities of LCB-RL sections with the proposed DSM curve

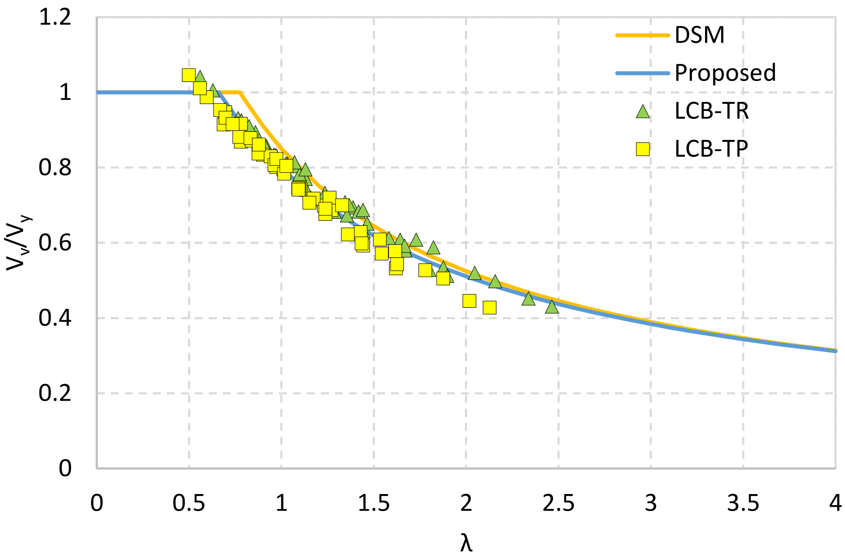

Fig. 17 Comparison of FE shear capacities of LCB-TR and LCB-TP sections with the proposed DSM curve

7.3 Reliability analysis

The capacity reduction factors were calculated for the proposed resistance models according to AISI S100 [12]. The method takes into account the effects of the uncertainties of the proposed resistance models, numerical models, geometric and material properties when determining the reduction factors. Eq. (28) is used to calculate the capacity reduction factor ($\emptyset_v$) in this method.

$$\emptyset_v = 1.52 M_m F_m P_m e^{-\beta_0 \sqrt{(V_m^2+V_f^2+C_p V_p^2+V_q^2)}} \tag{28}$$

where

M_m=1.1 is the mean of the material factor

V_m=0.1 is the variation coefficient of the material factor

F_m=1.0 is the mean of the fabrication factor

V_f=0.05 is the variation coefficient of the fabrication factor

P_m is the mean of the actual to predicted resistance ratio

V_p is the variation coefficient of the actual to predicted resistance ratio (not less than 0.065)

β_0 is the target reliability index

V_q=0.21 is the variation coefficient of the load effect

C_p is the correction factor and is given by Eq. (29).

$$C_P = \left[1 + \frac{1}{n}\right]\left[\frac{m}{m-2}\right] \tag{29}$$

where 'n' is the number of data points and m=n-1 is the number of degrees of freedom.

The capacity reduction factors for the proposed EN1993-1-4 [5] and the DSM resistance models were calculated and are given in Table 8. The target reliability index, β_0 was taken as 2.5 for all the cases. The minimum recommended value was used for the variation coefficient, V_p since the calculated values are less than 0.065 for all the resistance models. From the results, a capacity reduction factor of 0.90 can be recommended for all the proposed resistance models.

Table 8 Reliability analysis results

	Proposed EN1993-1-4 [5] resistance models		Proposed DSM resistance models	
	Eqs. (14)-(16)	Eqs. (17)-(19)	Eqs. (24) & (25)	Eqs. (26) & (27)
Capacity reduction factor (Ø_v)	0.901	0.902	0.901	0.902

8 Concluding remarks

The use of numerical modelling to investigate the shear response of cold-formed stainless steel LCB sections with longitudinal stiffeners was discussed. First, the developed FE models were validated with the shear tests of cold-formed stainless steel LCB sections found in the literature. Then, the elaborated FE models were utilised to study the shear behaviour of stiffened LCB sections in the numerical parametric study. The effect of return lips, and triangular and trapezoidal web stiffeners on the shear behaviour of LCB sections were comprehensively investigated for different stainless steel grades by generating a database of 144 FE models. Additionally, elastic shear buckling analyses were conducted for considered varying cross-sections using numerical modelling and shear buckling coefficients were back-calculated from the FE results.

From the observations of the shear buckling analysis, it was found that the back-calculated shear buckling coefficients (k_v) of LCB sections with return lips are almost equal to that of plain LCB sections. The back-calculated coefficients for LCB sections with web stiffeners are significantly higher compared to plain LCB sections where the sections with trapezoidal web stiffeners feature the highest coefficients among considered sections. Furthermore, it was concluded that the higher the indent of the web stiffener is, the higher the shear buckling coefficient. The observed shear buckling modes of LCB sections with return lips are found to be similar to that of plain LCB sections with single buckling half-waves while sections with web stiffeners have two buckling half-waves reducing the length of buckling half-waves. The spreading of the buckling half-waves over the whole web region was further observed, even with the presence of the web stiffeners.

It can be seen from the analysis of the shear failure modes of stiffened LCB sections that the buckling of web stiffeners located above the neutral axis of the section. Therefore, it was concluded that the stiffness of the longitudinal web stiffeners is not large enough to resist the out-of-plane buckling caused by the compressive stresses in the sections. Furthermore, it was observed that the shear capacity increment of the LCB sections with stiffeners is not significant compared to the plain LCB sections.

The evaluation of EN1993-1-4 [5] and the DSM shear design provisions suggested that the codified rules are conservative for cold-formed stainless steel LCB sections with return lips. Further, it was found that EN1993-1-4 [5] provisions over predict the shear capacities of LCB sections with trapezoidal web stiffeners while the DSM provisions over predict the shear capacities of LCB sections with both triangular and trapezoidal web stiffeners. Therefore, new provisions were proposed for EN1993-1-4 [5] web shear buckling reduction factor (χ_w) and the DSM shear design rules considering the FE results. The proposed design provisions provide enhanced shear resistance predictions with higher accuracy compared to the codified provisions.

Acknowledgements

Authors would like to thank Northumbria University for financial support and providing the necessary research facilities to conduct this research.

References

[1] C. H. Pham, L. A. Bruneau, G. J. Hancock, Experimental study of longitudinally stiffened web channels subjected to Combined Bending and Shear, J. Struct. Eng. 141 (11) (2015).

[2] C. H. Pham, G. J. Hancock, Direct strength design of cold-formed C-sections for shear and combined actions, J. Struct. Eng. 138 (6) (2012) pp. 759–768.

[3] L. Wang, B. Young, Design of cold-formed steel channels with stiffened webs subjected to bending, Thin-Walled Struct. 85 (2014) pp. 81–92.

[4] S. H. Pham, C. H. Pham, G. J. Hancock, Direct strength method of design for shear including sections with longitudinal web stiffeners, Thin-Walled Struct. 81 (2014) pp. 19–28.

[5] EN 1993-1-4:2006+A1:2015, Eurocode 3 – Design of steel structures – Part 1–4: General rules – Supplementary rules for stainless steels, European Committee for Standardization (CEN), Brussels, 2015.

[6] EN 1993-1-5, Eurocode 3 – Design of steel structures – Part 1–5: Plated structural elements, European Committee for Standardization (CEN), Brussels, 2006.

[7] T. Höglund, Behaviour and strength of the web of thin plate I-girders, Bulletin No. 93 of the Division of Building Statics and Structural Engineering, The Royal Institute of Technology, Stockholm, Sweden, 1971, pp. 13–30.

[8] O. Zhao, S. Afshan, L. Gardner, Structural response and continuous strength method design of slender stainless steel cross-sections, Eng. Struct. 140 (2017) pp. 14–25.

[9] B. W. Schafer, S. Ádány, Buckling analysis of cold-formed steel members using CUFSM: conventional and constrained finite strip methods, Proceedings of the eighteenth international speciality conference on cold-formed steel structures, Orlando, USA, 2006.

[10] V. V. Nguyen, G. J. Hancock, C. H. Pham, Development of the Thin-Wall-2 program for buckling analysis of thin-walled sections under generalised loading, Proceedings of the eighth international conference on advances in steel structures, Lisbon, Portugal, 2015.

[11] AS/NZS 4600, Cold-formed steel structures, Standards Australia/Standards New Zealand (AS/NZS), Sydney, 2018.

[12] AISI S100–16, North American Specification for the design of cold-formed steel structural members, American Iron and Steel Institute (AISI), Washington, 2016.

[13] D. M. M. P. Dissanayake, K. Poologanathan, S. Gunalan, K. D. Tsavdaridis, B. Nagaratnam, K. S. Wanniarachchi, Numerical modelling and shear design rules of stainless steel lipped channel sections, J. Constr. Steel Res. (2019) (In press).

[14] P. Keerthan, M. Mahendran, Experimental investigation and design of lipped channel beams in shear, Thin-Walled Struct. 86 (2015) pp. 174–184.

[15] P. Keerthan, M. Mahendran, Experimental studies on the shear behaviour and strength of LiteSteel beams, Eng. Struct. 32 (10) (2010) pp. 3235–3247.

[16] P. Keerthan, M. Mahendran, Shear behaviour and strength of LiteSteel beams with web openings, Adv. Struct. Eng. 15 (2) (2012) pp. 171–184.

[17] M. Mahendran, P. Keerthan, Experimental studies of the shear behavior and strength of LiteSteel beams with stiffened web openings, Eng. Struct. 49 (2013) pp. 840–854.

[18] ABAQUS 6.14 Analysis User's Guide, Dassault Systèmes, Rhode Island, USA, 2014.

[19] C. H. Pham, G. J. Hancock, Numerical simulation of high strength cold-formed purlins in combined bending and shear, J. Constr. Steel Res. 66 (10) (2010) pp. 1205–1217.

[20] P. Keerthan, M. Mahendran, Numerical modeling of LiteSteel beams subject to shear, J. Struct. Eng. 137 (12) (2011) pp. 1428–1439.

[21] P. Keerthan, M. Mahendran, D. Hughes, Numerical studies and design of hollow flange channel beams subject to combined bending and shear actions, Eng. Struct. 75 (2014) pp. 197–212.

[22] C. H. Pham, G. J. Hancock, Numerical investigation of longitudinally stiffened web channels predominantly in shear, Thin-Walled Struct. 86 (2015) pp. 47–55.

[23] J. K. Sonu, K. D. Singh, Shear characteristics of Lean Duplex Stainless Steel (LDSS) rectangular hollow beams, Structures 10 (2016) pp. 13–29.

[24] I. Arrayago, E. Real, L. Gardner, Description of stress-strain curves for stainless steel alloys, Mater. Des. 87 (2015) pp. 540–552.

[25] R. B. Cruise, L. Gardner, Strength enhancements induced during cold forming of stainless steel sections, J. Constr. Steel Res. 64 (11) (2008) pp. 1310–1316.

[26] M. Ashraf, L. Gardner, D. A. Nethercot, Strength enhancement of the corner regions of stainless steel cross-sections, J. Constr. Steel Res. 61 (1) (2005) pp. 37–52.

[27] R. G. Dawson, A. C. Walker, Post-buckling of geometrically imperfect plates, J. Struct. Div. 98 (1) (1972) pp. 75–94.

[28] L. Gardner, D. A. Nethercot, Numerical modeling of stainless steel structural components—A consistent approach, J. Struct. Eng. 130 (10) (2004) pp. 1586–1601.

[29] EN 1993-1-3, Eurocode 3 – Design of steel structures – Part 1–3: General rules – Supplementary rules for cold-formed members and sheeting, European Committee for Standardization (CEN), Brussels, 2006.

[30] C. H. Pham, G. J. Hancock, Shear buckling of channels using the Semi-Analytical and Spline Finite Strip Methods, J. Constr. Steel Res. 90 (2013) pp. 42–48.

[31] G. J. Hancock, C. H. Pham, Shear buckling of channel sections with simply supported ends using the Semi-Analytical Finite Strip Method, Thin-Walled Struct. 71 (2013) pp. 72–80.

[32] P. Keerthan, M. Mahendran, Shear buckling characteristics of cold-formed steel channel beams, Int. J. Steel Struct. 13 (3) (2013) pp. 385–399.

[33] P. Keerthan, M. Mahendran, Improved shear design rules of cold-formed steel beams, Eng. Struct. 99 (2015) pp. 603–615.

[34] S. Timoshenko, J. Gere, Theory of Elastic Stability, McGraw Hill, New York, USA, 1961.